JOURNAL OF MATERIALS SCIENCE 19 (1984) 2989–2996

Characterization of striations in polyethylene single crystals

A. BOUDET
Laboratoire d'Optique Electronique du CNRS, 29, rue Jeanne Marvig, F-31055 Toulouse Cedex, France*

New observations of polyethylene single crystals by electron microscopy are reported. Systematic studies of the contrast of striations and bend contours in bright and dark fields have been carried out. It is confirmed that bend contours are related to corrugations of the crystal. When rolled, these corrugations are changed into pleats. The quantity of extramaterial out of the substrate plane has been evaluated with the aid of the dynamical theory of contrast. Striations appear in the flat area and are proved to be due to local rotation and shearing of crystallographic planes. The change of contrast due to radiation damage is depicted and assigned to cross-linking in preferential planes which glide. The previous model of Bassett *et al.* of an initially non-flat-based pyramid-shaped crystal that coalesces to form corrugations is appropriate but the crystallographic characteristics must be changed to fit our observations and we propose another structure.

1. Introduction

Striations in polyethylene single crystals have already been observed by Bassett, Keller and coworkers [1–7], Reneker and Geil [8] and White [9] both by electron and light microscopy. In electron microscopy, they appear in bright or dark fields as long parallel lines, fairly straight, but sometimes waving and their direction changes in the vicinity of imperfections of the crystal [2, 5]. They can be permanent features [8] or transient and they disappear when the crystals dry [2]. Their most striking characteristic is the regularity of their directions. All authors agree on the {1 3 0} direction, but sometimes {2 5 0} and {1 2 0} are mentioned [3] or {5 3 0} [7]. This pattern of striations reveals the different sectors and was the principal argument for the sectorization of the crystal.

In dark fields the striations are identified as Bragg fringes [3, 8], disappearing under the flow of electrons that destroys the crystallinity [5]. The crystallographic planes are brought into the Bragg position when they are distorted in corrugations of the crystal, as revealed by shadowing.

There is evidence that these corrugations arise from the coalescence of an originally pyramid-shaped crystal [5]. The existence of a central pleat in the flat crystal and the changes of diffraction pattern from one sector to another prove that each sector has a different orientation. Ridges are formed when they dry. However, striated crystals can be observed when still in suspension [7]. In this case, ridges should appear during the growth of the crystal.

In dark-field images formed with a 1 1 0 beam, striations are visible only in the two (1 1 0) and ($\bar{1}\,\bar{1}$ 0) sectors – that is the sectors that are limited by the (1 1 0) and ($\bar{1}\,\bar{1}$ 0) growth faces – while they are present in four sectors in a 2 0 0 dark-field image.

In view of the variability of these observations, different models have been proposed to explain the mechanism of striation formation. On the basis of particular diffraction patterns, White interprets them as {1 3 0} twins [9]. Bassett *et al.* [7] believe the ridges are produced by a shear of the molecules along their axes during collapse of a pyramid. However, this mechanism does not cause any

*Laboratoire associé à l'Université Paul Sabatier.

0022–2461/84 $03.00 + .12

contrast so that it should be assumed that an additional deformation (the authors give no information about it) rotates the planes into the Bragg position.

During our observations of polyethylene single crystals for a detailed work on diffraction [14], we had the opportunity to use various techniques in electron microscopy and we found measures that were not consistent with previous models. We then went on to modify the model of Bassett *et al.* to fit the results for our crystals and we noticed additional characteristics on the figure of striations and on the effect of radiation damage. These observations are reported here.

2. Experimental details

The polyethylene single crystals are obtained by growth in a dilute (0.01%) solution of Manolene ($M_n = 11\,000$, $M_w = 90\,000$) in tetrachloroethylene, using the self-seeding method [10]. By slightly changing the solution used and the experimental conditions, sizes ranging between 8 and 80 μm are obtained. A droplet of the solution is spread out on a carbon film deposited on a copper grid.

TEM observations were performed at 100 kV or higher (1 to 2 MV) voltages. Since these specimens are highly beam-sensitive, several techniques have been used in order to minimize the damage and increase the lifetime. At 100 kV the beam intensity used was 0.1 A m^{-2} so that the image obtained on the screen was hardly visible and could only be checked by an eye adapted to the darkness or with the help of an image intensifier. Recordings were made on high speed films (Kodirex). Increasing the accelerating voltage improves the lifetime, so the high voltage electron microscope of the laboratory was connected to an image intensifier, images being also recorded on Kodirex films.

With help of such procedures, dark- and bright-field images and diffraction patterns of almost non-irradiated crystals could be obtained.

The structure and the geometry of the crystal is shown in Fig. 1. Each side of the crystal is a {1 1 0} growth face parallel to the folding plane of the polyethylene chains. The chains are parallel to the c-axis of the unit cell [11].

3. Observation of extinction contours

In dark-field images we observed more or less regular fine white lines depending upon the way the crystals were prepared (Figs. 2 and 3, Figs. 1 to 3 of [12], Fig. 3 of [13], Plate I of [14]).

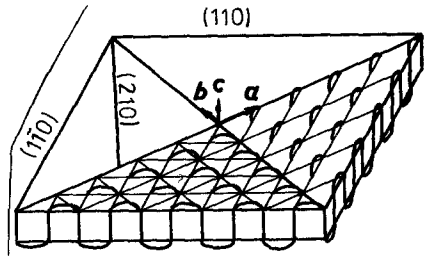

Figure 1 Structure and geometry of a perfect polyethylene single crystal.

3.1. Characteristics of the contours

In most simple crystals the contours were almost straight, but they followed irregularities in larger crystals, due to relief, folds or bubbles. They can be either isolated and rare or numerous or even missing. They can also be ribbon-like. Their width was measured to be 10 nm on average and sometimes reached 50 or 60 nm. Their direction, oblique with respect to the growth faces of the crystal and symmetrical with respect to the diagonals, cannot be given crystallographic indices.

Some crystals were examined both by electron microscopy and light microscopy in phase contrast and Nomarski contrast and it could be established that these lines were extinction contours related to corrugations of the crystals, the width of which was estimated to be 2.5 μm (Fig. 4).

3.2. Contrast of the extinction contours

In 200 dark-field images, contours were present in four sectors of the crystal but only in two sectors with (1 1 0) growth faces in a 1 1 0 dark-field image (see Plate I of [14]). When the crystal was tilted, the loops of the contours became larger or smaller.

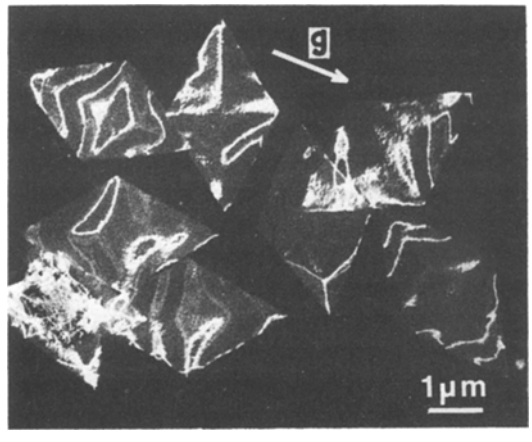

Figure 2 Extinction contours, dark-field image, 1500 kV.

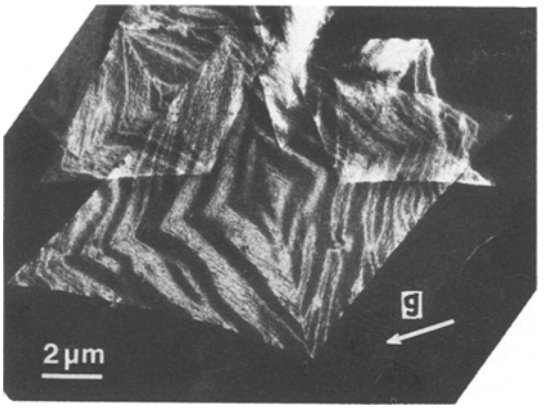

Figure 3 Extinction contours, 2 0 0 dark-field image, 1500 kV.

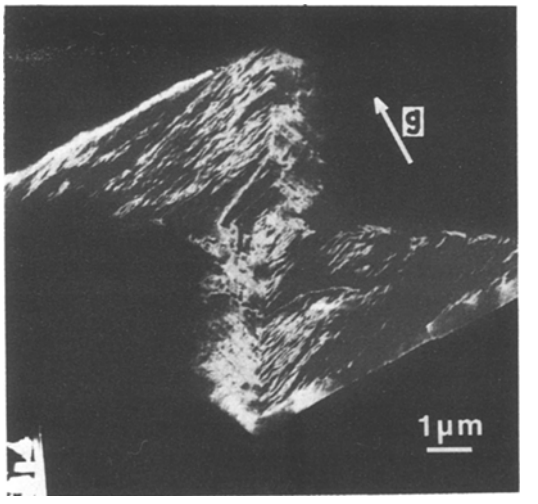

Figure 4 Extinction contours related to a fold along the small diagonal. 1 1 0 dark-field image, 100 kV.

This observation is explained in Fig. 5. This figure and Fig. 6 show how the (1 1 0) planes in the (1 1 0) faced sectors, almost parallel to the corrugations, are strongly disoriented and give extinction contours while the (1 $\bar{1}$ 0) planes in the same sectors, almost perpendicular to the corrugations, are not disturbed.

3.3. Further coalescence of the corrugations

When the crystal was irradiated by the electron beam, dark lines appeared in the bright-field indicating that the initial corrugations had coalesced into several pleats (Fig. 7) while the crystallinity was destroyed and the extinction contours vanished (see [12]). Shadowing produces a similar effect and the pleats can be measured (Fig. 8): height 20 to 40 nm; width 20 to 50 nm; oblique direction with respect to growth faces of the crystal.

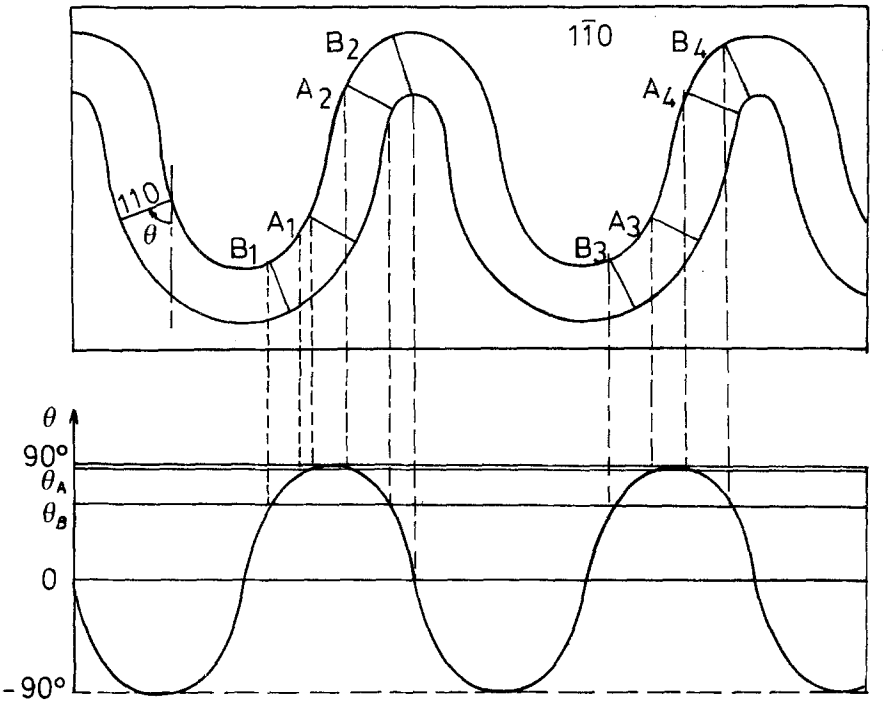

Figure 5 (a) Formation of folds by rotation of (1 1 0) planes. The (1 $\bar{1}$ 0) planes remain nearly undisturbed. (b) The change in contours when the incident angle is varied.

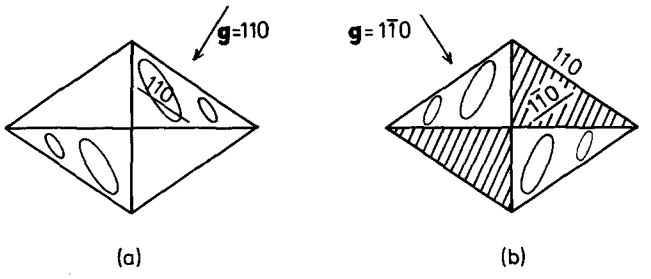

Figure 6 Contrast of extinction contours: (a) 1 1 0 dark-field image; (b) 1 $\bar{1}$ 0 dark-field image with 1 1 0 and $\bar{1}$ 1 0 faced sectors in the Bragg position.

The extinction contours are thus evidence of a rotation of the (1 1 0) planes due to corrugations, and the pleats resulting from the coalescence of the corrugations have been measured. This leads us to a precise evaluation of the original pyramid shape in Section 5.

4. Observation of striations

Other crystals had a quite different appearance and are crossed by striations as shown in Fig. 9 and in Fig. 1–2 of [13]. In these crystals extinction contours were not found. Striations and contours had a similar contrast in dark-field images but the characteristics of the striations differed on several points.

4.1. Size

The width of striations remained constant on the same line: 20 to 60 nm, but the distance between them was 40 to 180 nm.

4.2. Direction

The direction of the striations was regular and crystallographic indices could be attributed: the angle between the striations of two adjacent sectors was measured on the micrographs and on laser diffractograms (see [15]). Its value of $98 \pm 3°$ is related to a ⟨3 5 0⟩ direction. As will be seen below (Section 5) this angle must be referred to a non-horizontal face of the pyramid so that the indices are changed into ⟨1 2 0⟩. Note that ⟨1 2 0⟩, as ⟨3 5 0⟩, are scarcely mentioned in the literature while they are present in all the striated crystals studied here.

4.3. Structure defects

When the crystal was tilted, striations were alternatively visible and not so, without moving; thus they are attributed to a local fault. They did not appear in 1 1 0 dark field in the $(\bar{1}\,\bar{1}\,\bar{0})$ faced sector. So, according to the rule $\mathbf{g} \cdot \mathbf{R} = 0$ [16], where $\mathbf{g}$ is the selected beam, the displacement vector $\mathbf{R}$ of the atoms lies in a (1 1 0) plane, nearly perpendicular to the striations. This seems to be a rotation of the $(1\,\bar{1}\,0)$ plane in the striation.

4.4. Effect of electron irradiation

When radiation damage occurred, the diffraction pattern first remained unchanged then disappeared [17]. At the same time, the contrast of striations first increased and then vanished (see [13]). The striations were clearly seen in a bright-field image on damaged crystals (Fig. 10 and Fig. 4 of [12]). The phase contrast presented here showed that

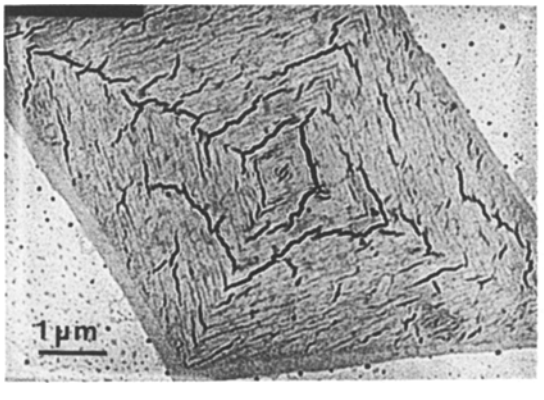

Figure 7 Folds of the damaged crystal; bright field, 100 kV.

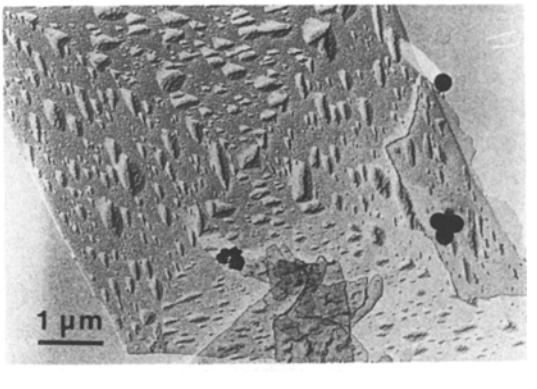

Figure 8 Chromium-shadowed crystal at 20° angle with latex balls. Bright field, 100 kV.

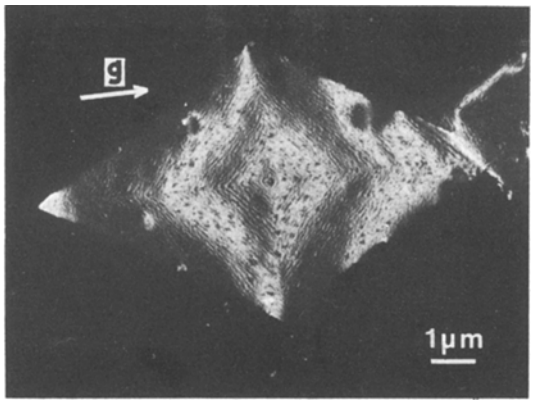

Figure 9 Striations; 2 0 0 dark field, 100 kV.

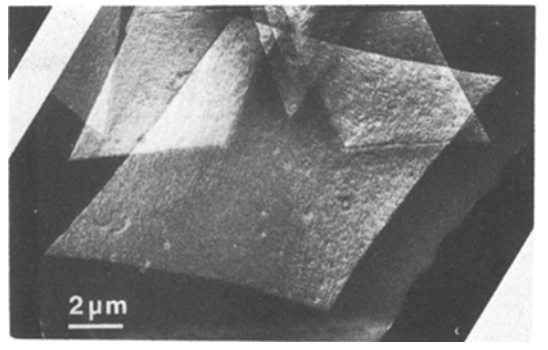

Figure 11 Same crystal as in Fig. 3 after radiation.

edges have been produced along striations. This seems to be the result of a shear in the vertical planes of the striations.

This process can be compared with radiation in metals where it has been shown that damage happens more intensively in distorted areas for some crystallographic orientations [18]. In our case cross-linking between the chains could take place in the planes of the striations (their projection being ⟨1 2 0⟩ and not between these planes so that they can glide and this shear creates small edges in agreement with the defocusing contrast of Fig. 10.

This aspect brings our striations close to the irradiation lines of Petermann and Gleiter [19] but they are, however, different because their lines are not present at the beginning of the observation, have [1 0 0] and [0 1 0] directions, and are not disturbed when crossing the diagonals.

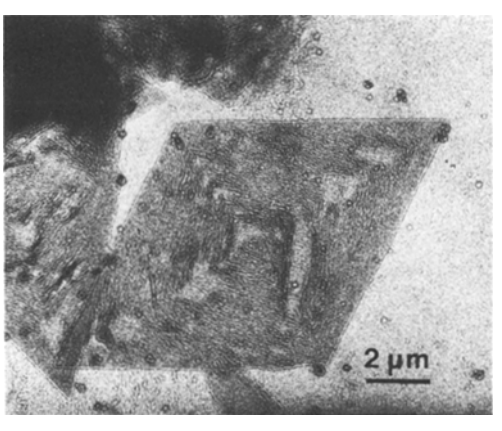

Figure 10 Striations, contrast enhanced by defocusing; bright field, 100 kV.

4.5. Effect of the method of preparation of the crystals: extinction contours and striations

When deposited on a glass slide with a pipette, the most simple small crystals had a single corrugation along the small diagonal (Fig. 4) with several extinction contours, but if the same crystals were rolled in order to spread them all over the slide, contours and the corrugation disappeared. The crystal was nearly flat with many striations and sometimes pleats. Striations are then due to the flattening of the initial corrugation.

Radiation damage has a similar effect: extinction contours are progressively replaced by striations, indicating that the crystal flattens when irradiated (Figs. 3 and 11).

The mechanism of coalescence will be specified in Section 6, when the initial shape of the crystals is indicated.

5. The initial pyramid shape of the crystals

Since publication of the papers of Bassett *et al.* [5–7], it is assumed that the crystals are non-flat-based pyramids and they coalesce to form corrugations. However, White [9] observed flat crystals and assigned striations to twins. Our crystals are different both from those of White and Bassett: bend contours and striations are seen separately in different conditions of preparation. So the initial shape and the contrasts of the crystal may vary largely according to the crystallization conditions and the preparation for electron microscopy. The non-flat-based pyramid shape that is suitable for other crystals must be justified for ours.

Note first that the model of White does not agree with our crystals as no double diffraction pattern can be seen as in twins.

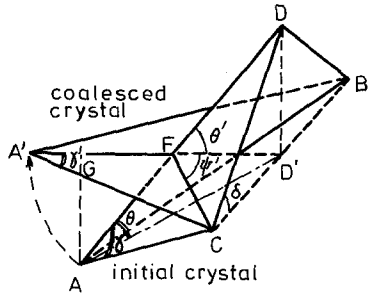

Figure 12 Model of the initial pyramid (only one half is represented).

5.1. The values of the crystal angles involved in a pyramid shape

If the crystal was flat, the angle γ' between the (1 1 0) growth faces of the crystal should be 67.5° and the ratio L/l of the lengths of the diagonals 1.5. The real values measured on our micrographs are, respectively, $\gamma' = 61.8 \pm 1.4°$ and $L/l = 1.67$, values scarcely reported for the crystals of other authors. Such an angle in a flat crystal would correspond to a ⟨10-9-0⟩ direction, physically impossible. In fact this angle γ' is the projection on the substrate plane of an angle $\gamma = 67.5°$ measured on the pyramid.

5.2. Non-flat-based pyramid (Fig. 12)

In this model, the molecules are vertical and the base is not a plane (Fig. 13). FC is fixed on the substrate. A section of the pyramid by the base plane passes through C. The coalescence can be artificially decomposed in two parts: AF is tilted into A'F in the base plane (Fig. 13); another part shears from FD to FD' (Fig. 14).

As GD'/CD' = 1.5 and A'D'/CD' = 1.67 (cf. Section 5.1), it can be calculated that:

$$\theta = 15°;\ \delta = 28°;\ \theta' = 35°;\ \psi' = 53° \quad (2)$$

In a crystal for which $L' = 5\,\mu m$, $h = 1.6\,\mu m$. The FC direction that appears as a ⟨3 5 0⟩ direction in the projected triangle A'D'C' is in reality a ⟨1 2 0⟩ when referred to the ADC triangle.

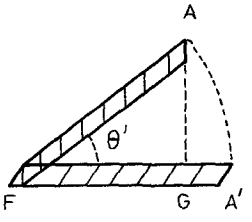

Figure 13 Rotation of the pyramid face.

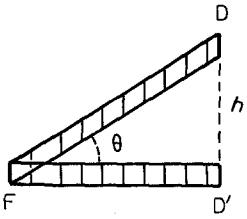

Figure 14 Shearing of the pyramid face.

These calculated values for θ and δ are in good agreement with the angles 18° and 26° measured by Bassett *et al.* in their study of the central pleat.

6. Coalescence mechanisms

6.1. The two possible mechanisms

In the first mechanism, the face rotates as a whole without any shear of the molecules (Fig. 13) and produces an excess of material in the base plane along the diagonal: $E = GA' = FA(1 - \cos\theta) = 0.57\,\mu m$ with the values calculated in Section 5.2. The second mechanism brings FD into the FD' position by a shear of the molecules (Fig. 14), does not produce any excess of materials and does not bring any change of contrast as does the first mechanism. Therefore, the first necessarily takes place, but the second is not excluded.

6.2. Estimation of excess material

The excess material can be estimated from the folds (for instance Fig. 8) or from a corrugation (Fig. 4). In Fig. 8, 12 folds 30 nm high are visible and represent approximately $E = 0.7\,\mu m$.

It is possible to obtain the radius of curvature of the corrugation from the rocking curve of the intensity of a diffracted beam at the back face of the specimen plotted against its thickness and orientation. We have calculated this by computer using the dynamical theory with 12 beams, knowing the atomic diffusion factors, for a thickness of 16 nm (Fig. 15) [16]. θ_B is the Bragg angle of the (1 1 0) planes. The intensity is at a maximum for $\theta = \theta_B$. The problem is knowing why the extinction contours of Section 3.1 have a finite width of 40 nm: we have established, using a microdensitometer, that the edges of such a line have an intensity equal to the background noise, the value of which is half the maximum intensity in the middle of the contours. In Fig. 15, we see that the difference of orientation, $\Delta\theta$, for half intensity corresponding to the width of the contour is $\Delta\theta = 4\theta_B = 0.02$ rad. Thus the radius of curvature, $R = 0.04/0.02 = 2\,\mu m$.

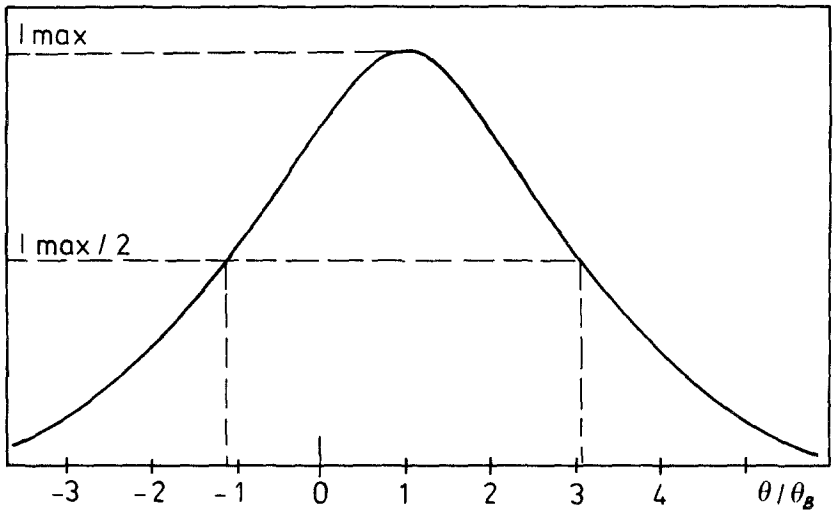

Figure 15 Rocking curve of extinction contours in polyethylene. 1 1 0 dark field; thickness 16 nm, 12 beam dynamical theory.

The excess of material, E, is the difference between the arc $R\alpha$ and the chord $2R \sin(\alpha/2)$. In Section 3.1, a corrugation with a 2.5 μm chord was found, that is $\alpha = 1.35$ rad and then $E = 0.2\,\mu$m. So three or four corrugations, as well as the approximately 12 folds mentioned above agree with the theoretical calculations.

The same calculation applied to the striations leads to a negligible excess of material $E = 0.01$ nm, for each striation. No relief is associated with the striation itself.

7. Conclusions

7.1. Initial shape of the pyramid

We examined here a non-flat-based pyramid, but the same work was also performed assuming a flat-based pyramid: the agreement is not so good with the measured angles and with the cell parameters as in the non-flat-based model. For this latter model, if we try to justify the angles θ' and δ from the structure of the cell, we find that they result from a vertical shift of the molecules parallel to their c-axis from one cell to another, the value of which is 2 c along the a-axis and c along the b axis (Fig. 16). So:

$$\theta' = \text{Arctan}\frac{2c}{a} = 34.4°$$

$$\delta = \text{Arctan}\frac{c}{b} = 27.2°$$

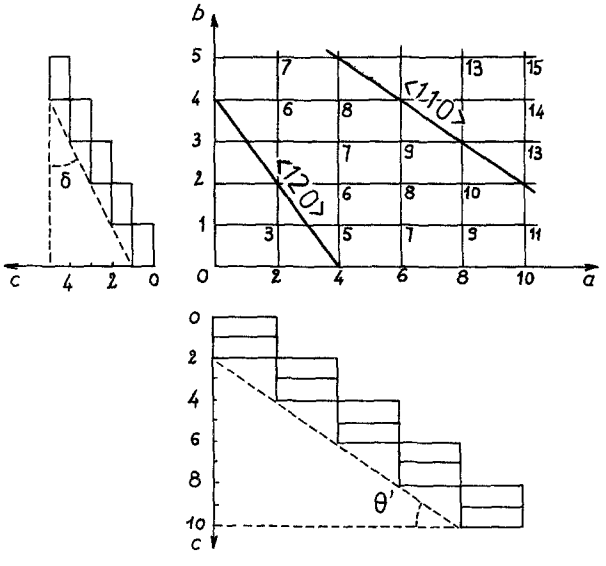

Figure 16 Structure of the pyramid faces; (2 1 1) plane. The numbers indicate the height under the apex in **c** unit. ⟨1 2 0⟩ lines represent the striations.

in excellent agreement with the values of our model $\theta' = 35°$ and $\delta = 28°$. This structure is plotted in Fig. 16. The molecules with an equal height above the basal plane are found on the $\langle 1\,2\,0 \rangle$ axis.

This model is similar to that of Keller [7] but differs on the following points:

1. striations have [1 2 0] directions and not [1 3 0];

2. the pyramid faces are (2 1 1) planes and not (3 1 4) or (3 1 2);

3. the shift along **c** is 2**c** and **c** instead of $\frac{3}{2}$**c** and $\frac{1}{2}$**c**.

These discrepancies do not imply that his model is wrong, but only that it is not applicable to our crystals: they may well be different from his own because of the mode of crystallization.

Our model disagrees with another model, that that proposed by Bassett [5], in which the distortion due to the folding of the chains gives rise to an acute angle in the cell. To match each other, the sides of the sectors must not be in the same plane. As the distortion is $4\theta = 0.5°$, it cannot be fitted with value of 24° calculated from our model. Furthermore, observation of rotation of terraces [20] suggests that the distortion angle is rather obtuse.

7.2 Corrugations and striations

When the pyramid coalesces gently, large corrugations are formed as indicated by the bend contours on the micrographs. We have shown that striations are due to a more pronounced coalescence when crystals are rolled. Then crystals become flat, the excess material is distributed into pleats instead of corrugations, and striations are tiny local folds or corrugations, associated with a rotation of (1 1 0) planes and shear of molecules in the (2 1 0) planes.

This more drastic coalescence imposes a crystallographic direction on the striations, the $\langle 1\,2\,0 \rangle$ direction, which is the line of intersection of the pyramid with the plane of the substrate.

7.3. Radiation damage

During radiation damage, the crystals become flat as for rolling, and corrugations are changed into striations and pleats. Striations become more marked, because there is a vertical shear in the (2 1 0) planes. Radiation damage seems to be favoured in these (2 1 0) planes during a channelling process that will be investigated in a subsequent paper, so that cross-linking takes place in them but not between them and they can glide easily along each other during radiation.

Acknowledgement

The author wishes to thank Dr B. Lotz (Centre de Recherches sur les Macromolécules, Strasbourg, France) for valuable discussions and encouragement.

References

1. D. C. BASSETT, F. C. FRANK and A. KELLER, *Nature* **12** (1959) 810.
2. A. W. AGAR, F. C. FRANK and A. KELLER, *Phil. Mag.* **4** (1959) 37.
3. D. C. BASSETT, F. C. FRANK and A. KELLER, in "Proceedings of the European Regional Conference on Electron Microscopy", Delft, August–September 1960, edited by A. L. Houwink and B. J. Spitt (de Nederlandse vereniging voor electronenmicroscopie, Delft, 1960) Vol. 1, p. 244.
4. A. KELLER, *Phil. Mag.* **6** (1961) 329.
5. D. C. BASSETT and A. KELLER, *ibid.* **6** (1961) 345.
6. D. C. BASSETT, F. C. FRANK and A. KELLER, *ibid.* **8** (1963) 1739.
7. *Idem, ibid.* **8** (1963) 1753.
8. D. H. RENEKER and P. H. GEIL, *J. Appl. Phys.* **31** (1960) 1916.
9. J. R. WHITE, *J. Mater. Sci.* **9** (1974) 1860.
10. D. J. BLUNDELL, A. KELLER and A. J. KOVACS, *J. Polymer Sci. B Polymer Lett.* **4** (1966) 481.
11. B. WUNDERLICH, "Macromolecules Physics" Academic Press, New York and London, 1973).
12. A. BOUDET and L. P. KUBIN, in "Electron Microscopy 1978", Ninth International Congress on Electron Microscopy, Toronto, Canada, August 1978, edited by J. M. Sturgess (Microscopical Society of Canada, Toronto, 1978) Vol. 1, p. 498.
13. *Idem*, in "Electron Microscopy 1980", Seventh European Congress on Electron Microscopy, The Hague, The Netherland, August 1980, edited by P. Brederoo and G. Boom (North-Holland, Amsterdam, 1980) Vol. 1, p. 434.
14. A. BOUDET and L. P. KUBIN, *J. Microsc. Spectrosc. Electron.* **5** (1980) 187.
15. A. BOUDET, Thèse de doctorat, Toulouse (1981).
16. P. H. HIRSCH, A. HOWIE, R. B. NICHOLSON, D. W. PASHLEY and M. J. WHELAN, "Electron Microscopy of thin Crystals" (Butterworths, London, 1965).
17. A. BOUDET and L. P. KUBIN, *Ultramicroscopy* **8** (1982) 409.
18. L. E. THOMAS, *Rad. Effects* **5** (1970) 183.
19. J. PETERMANN and H. GLEITER, *Kolloid Z. Z. Polymere* **251** (1973) 850.
20. J. RAULT, *J. Macromol. Sci. Phys. B* **12** (1976) 335.

Received 4 July
and accepted 29 November 1983